Soft Matter

Accepted Manuscript

ROYAL SOCIETY OF CHEMISTRY

www.rsc.org/softmatter

Model of vesicle tubulation and pearling induced by adsorbing particles

Yu-Cheng Su[a] **and Jeff Z. Y. Chen** *[a]

Received Xth XXXXXXXXXX 20XX, Accepted Xth XXXXXXXXX 20XX
First published on the web Xth XXXXXXXXXX 200X
DOI: 10.1039/b000000x

We study a basic theoretical model for a deformable vesicle immersed in a solution of particles that can adsorb to one of the two surfaces of a membrane. The model consists of an adsorption energy gain for the adsorbing particles and the Canham-Helfrich membrane bending energy, in which the spontaneous curvature is coupled with the adsorption area. We demonstrate that bud, pearling, and tube conformations can be stabilized after minimizing the free energy and that the pearling-tubulation transition has the characteristics of an abrupt structural transition.

1 Introduction

In recent years, significant theoretical and experimental attentions have been directed towards understanding the morphology formed by fluid membranes that interact with other molecules. A challenge is to provide a fundamental explanation of the rather simple structural formation in real soft-matter and biological systems which otherwise have a highly complex molecular nature [1–19]. While budding, tubulation and pearling are ubiquitously seen in biological systems, the mechanisms that lead to these structural formations have long been the subject of carefully designed biophysical experiments which targeted at cell-shape instability by changing biological or physical conditions [2,4,5,15,20–22]. Experiments have shown that when a membrane surface is collectively modified in the form of molecular insertion into the lipid bilayer or multi-particle adsorption on the lipid surface, extraordinary tubulation and pearling transitions can occur in a membrane system on a length scale much greater than the modifying-particle size [4,5,15,22]. Hydrophilic polymers with hydrophobic side groups, for example, were used as anchors to modify the outer monolayer of a membrane tube or vesicle and to induce shape instability [4,5,23]. Alternatively, cationic nanoparticles encapsulated within DOPC vesicles can modify the inner monolayer and produce tubulation and pearling [15].

Theoretically, the profound structural properties in these systems are usually discussed in the context of coarse-grained models with a few key physical parameters to capture the basic mechanisms [24,25]. The Helfrich curvature energy was previously analyzed for a *single*-component vesicle to yield conformations containing a large mother cell connected to several smaller cells, with and without additional area-difference

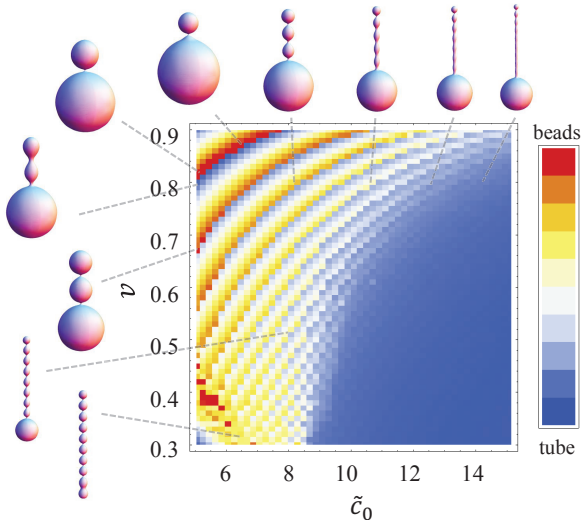

Fig. 1 Shape diagram in terms of the reduced vesicle volume v and adsorption-induced spontaneous-curvature coupling parameter $\tilde{c}_0$ with a fixed reduced chemical potential $\tilde{\mu} = -5.1$, yielded from this work. The diagram is colored according to the shape parameter γ defined in the text; a high γ (red) indicates the formation of one or several pearl beads; a low γ (blue) indicates a tubular protrusion. Each band from blue, white, to red (or yellow) contains a particular number of beads within the protrusion.

[a] *Department of Physics and Astronomy, University of Waterloo, Waterloo, Ontario, Canada, N2L 3G1. E-mail: jeffchen@uwaterloo.ca*

considerations, for membranes preferring a spontaneous curvature[26–28]. In addition, the generalization of the models to account for the difference in spontaneous curvatures of *two*-component vesicles is also possible, where the spontaneous curvature is assumed to be linearly coupled to the composition density[26,28,29]; a budding state, for example, can be established through such a model[30]. While the membrane pearling instability has been theoretically explored in other context[20,31,32], here we aim at understanding the curvature-generating and adhering-particle aggregation mechanisms for particle-adhering vesicles[4,33,34]. The model contains two fundamental energetic terms: the Canham-Helfrich bending energy for the membrane and an adsorption energy term for the adhering particles, applicable when the adsorption energy dominates over the entropic effects of the adhering particles. It is much simpler than those proposed to study tubulation and pearling due to particle anchoring[4,33,34]. Simultaneously treating coupled vesicle deformation and particle adsorption, we show the existence of tubular structures with a hint of pearling formation, which are seen experimentally but not previously determined in either *single*- or *two*-component vesicle models. An example of the calculated structural properties can be viewed in Fig. 1.

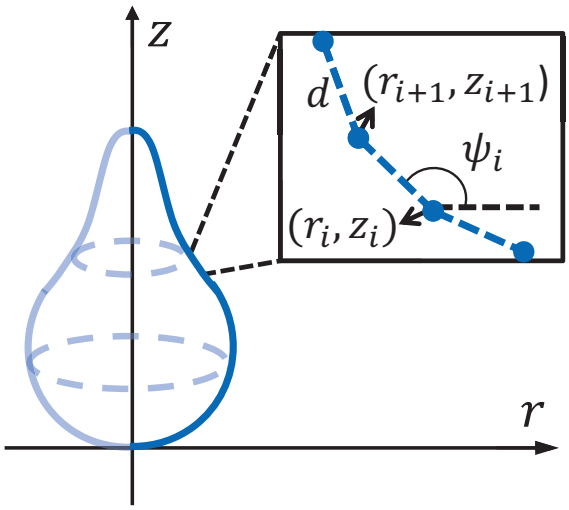

Fig. 2 Discretization scheme of the shape curve representing the vesicle in an axisymmetric setting. The curve is discretized into N nodes by a distance d. Variables r_k and ψ_k ($k = 1, 2, ..., N$) were treated as independent variables in our minimization scheme.

2 Model

We consider a vesicle surface, where one side, either exterior or interior, is in contact with a particle solution. No interaction between these particles themselves is considered. They can adsorb onto the surface of a membrane due to a short-range surface force. All length variables are reduced by the factor

$$R = (A/4\pi)^{1/2} \tag{1}$$

where A is the vesicle surface area. The total reduced free energy F is then

$$\frac{F}{\kappa} = \frac{1}{2}\int \left[2\tilde{M} - \tilde{c}_0\phi(\mathbf{x})\right]^2 \mathrm{d}\tilde{A} + \tilde{\mu}\int \phi(\mathbf{x})\mathrm{d}\tilde{A}, \tag{2}$$

where $\tilde{c}_0 = c_0 R$, $\tilde{\mu} = \mu R^2/\kappa$, $\tilde{M} = MR$ and $\mathrm{d}\tilde{A} = \mathrm{d}A/R^2$. Here, the area fraction covered by adsorbing particles, $\phi(\mathbf{x})$, is coupled to the spontaneous curvature by c_0[35]. The first term is the Canham-Helfrich energy which contains the mean curvature M for a surface element $\mathrm{d}A$[36,37]. The particle adsorbing chemical potential, μ, is reduced by the bending energy modulus κ. The model is suitable for a system with strong adsorption such that the entropy of the adsorbing particles can be ignored. In addition, we assume that the closed two-dimensional vesicle has a constant surface area A and constant internal volume V, subject to shape deformation. Mathematically, two constraints need to be invoked, as customarily considered in previous studies[38]. The relaxation of the volume constraint will be discussed later for a solvent-permeable vesicle. The model contains three basic parameters: the reduced vesicle volume

$$v = 3V/4\pi R^3, \tag{3}$$

$\tilde{c}_0$, and $\tilde{\mu}$. Here we ignore the thermal fluctuations of the membrane and take the conformation corresponding to the free-energy minimum as the stable state[24,25].

3 Numerical scheme

In previous treatments on related membrane models where both physical properties were considered, the membrane shape was determined according to an *a priori* assumption that the area fraction $\phi(\mathbf{x})$ has a specific function form[33,34,39–43]. Here, for a deformable vesicle that has an axisymmetric shape about the z axis, we introduced a shape function, $r(s)$ and $z(s)$, where s is the arcvariable along the shape, together with an axisymmetric distribution $\phi(s)$. Minimization of F with respect to all three functions was performed simultaneously, subject to energy penalty terms that deal with the constraints in the system[44,45].

In our numerical procedure, the curve is discretized into N nodes, each separated by an equal distance d. We further introduce an angle variable ψ, the angle between the neighboring nodes and the horizontal line. The coordinates r and z depend

on ψ through

$$r_{i+1} = r_i + d\cos\psi_i, \quad (4)$$
$$z_{i+1} = z_i + d\sin\psi_i, \quad (5)$$

where i is the node index. This discretization scheme is illustrated in Fig. 2. With axisymmetry the adsorption of particles onto the membrane surface is described by the area fraction $\phi(s)$ as a function of the arcvariable s. We also discretize $\phi(s)$ into ϕ_i for node i under the constraint $0 \le \phi_i \le 1$.

The approach of solving the Euler-Lagrange equation for the shape functions was taken previously[25,38,46–48], where the mathematical constraints on the total surface area and total internal volume were incorporated through the Lagrange multipliers. In the current work, we take a different numerical approach, in which all mathematical constraints such as the total area, total volume, and the r_i-ψ_i relation in Eq. 4 are expressed by energy penalty terms[44,45]. We introduce a dimensionless target function using a discretized form of Eq. (2),

$$\begin{aligned}\frac{F}{\kappa} =& \tilde{F}[\{\psi_i\},\{r_i\},\{\phi_i\};d] \\ =& \frac{1}{2}\sum_i \Big[\frac{\psi_{i+1}-\psi_i}{d} + \frac{\sin\psi_i}{r_i} - \tilde{c}_0\phi_i\Big]^2 \Delta A_i \\ &+ \tilde{\mu}\sum_i \phi_i \Delta A_i \\ &+ \Lambda_A\Big[1 - \frac{1}{4\pi}\sum_i \Delta A_i\Big]^2 \\ &+ \Lambda_V\Big[1 - \frac{3}{4v}\sum_i \Big(\frac{r_{i+1}+r_i}{2}\Big)^2 d\sin\psi_i\Big]^2 \\ &+ \Lambda_d \sum_i (r_{i+1} - r_i - d\cos\psi_i)^2,\end{aligned} \quad (6)$$

where

$$\Delta A_i = \pi d(r_{i+1} + r_i). \quad (7)$$

The terms with coefficients Λ_A and Λ_V reproduce the area and volume constraints and force the reduced volume at v; the last term with a prefactor Λ_d were introduced because $\{r_i\}$ and $\{\psi_i\}$ are treated as independent variables in our minimization scheme. We increase Λ_A, Λ_V, and Λ_d until a satisfactory numerical precision is achieved.

For a fixed set of $\tilde{c}_0$, $\tilde{\mu}$, and v, within an iteration step, we numerically minimized the target function, treating it as a multi-variable minimization problem that can be efficiently dealt with by the L-BFGS-B algorithm[49]. At the next iteration step, the penalty factors Λ_A, Λ_V, Λ_d were increased by one percent, starting from 500 to arrive at a final 10^7. The error tolerance of the minimization was selected such that the contribution of the penalty terms was less than 0.1 percent to the final minimized target function. In order to test the numerical scheme, we enforced $\tilde{c}_0 = \tilde{\mu} = 0$ to reproduce

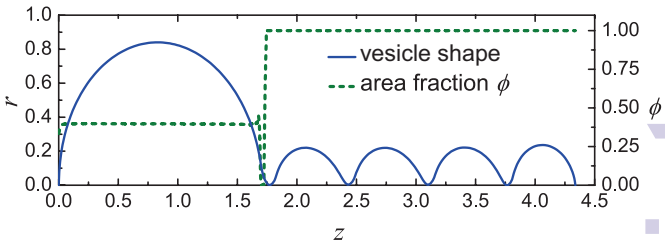

Fig. 3 Optimized shape function for a system at $\tilde{c}_0 = 7.6$, $\tilde{\mu} = -0.51$ and $v = 0.70$. To the left scale, the solid curve illustrates the vesicle shape; to the right the dashed curve represents the adsorption area fraction ϕ. Note that r and z are reduced by the factor R given in the text.

the stability regions of typical vesicle conformations. We can show that the prolate conformation is stable within the region $v = (0.65, 1.0]$, the oblate conformation is stable within the region $v = (0.59, 0.65]$ and the stomatocyte conformation is stable within the region $v = (0.0, 0.59]$, which can be compared with the previous results $v = [0.652, 1.0]$, $v = [0.592, 0.651]$, and $v = (0.0, 0.591]$ for these phases determined by Seifert *et al.* using a different numerical technique[38]. All numerical results in the current paper are based on $N = 301$.

To demonstrate the coupling among $r(s)$, $z(s)$ and $\phi(s)$, in Fig. 3 an example is displayed, containing an almost spherical mother vesicle, and a protrusion. The latter is an almost uniform string of pearls, in connection with a constant $\phi = 1$ over the entire region — adsorbing particles aggregate in this region. The radius of a pearl bead is close to $2/\tilde{c}_0$. Hence we can estimate $\tilde{c}_0$ in an experiment by the observed bead size. In both pearling experiments of a nanoparticle-adsorbing giant unilamellar vesicle (GUV)[15] and a polymer-anchoring tubular phospholipid membrane[4], no evidence of nonuniform accumulation of adsorbing molecules at regions with different curvatures was found when the entire system transformed into a string of pearl beads; our result is consistent with the experimental observations. However, within the mother vesicle region, $\phi(s)$ is approximately a constant less than 1. Near the neck connecting the protrusion and the mother vesicle, $\phi(s)$ decreases sharply to 0 at the location where vesicle has a mean curvature 0, displaying a catenoid shape. This was also seen in Ref. 30 based on a different model.

4 Protrusion conformation

A shape parameter γ is defined to measure the conformation in the protrusion,

$$\gamma = \frac{\langle r\rangle - 1/\tilde{c}_0}{\pi/(2\tilde{c}_0) - 1/\tilde{c}_0}, \quad (8)$$

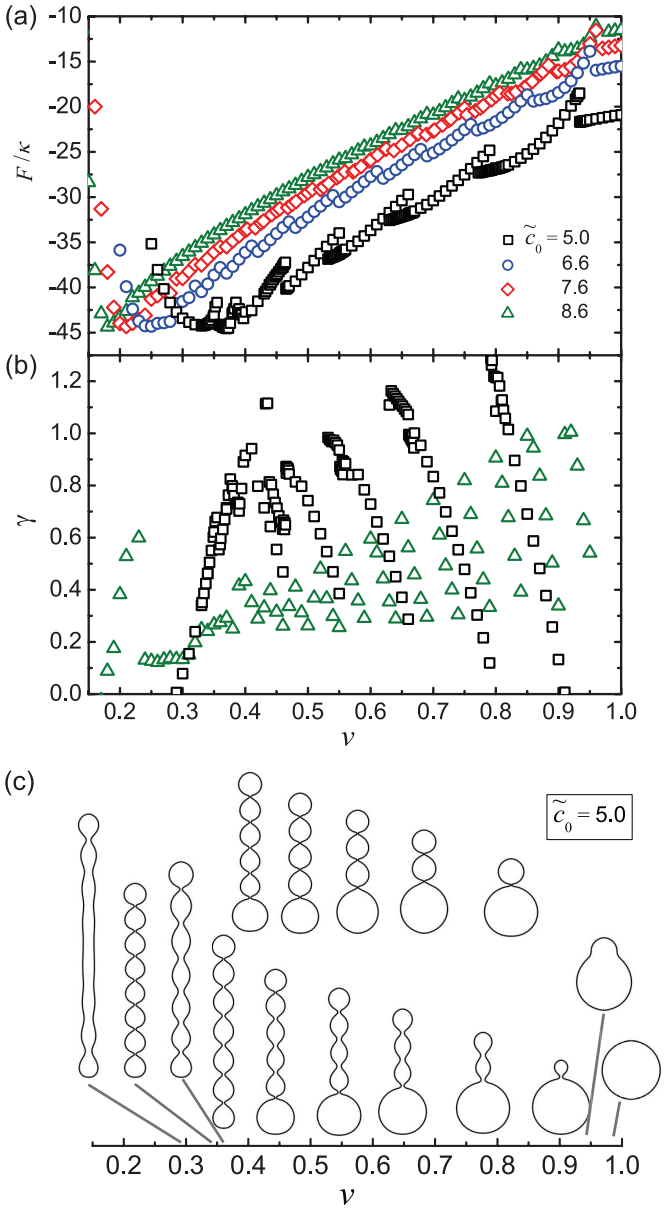

Fig. 4 (a) Total energy F as a function of v for systems having $\tilde{\mu} = -3.56$ and various $\tilde{c}_0$. As two neighboring branches of F cross, the system undergoes an abrupt shape transition between shapes having different number of pearling beads. (b) Shape parameter γ as a function of v and (c) Membrane shape as a function of v for $\tilde{\mu} = -3.56$ and $\tilde{c}_0 = 5.0$.

where $\langle r \rangle \equiv \int r(s)\mathrm{d}A / \int \mathrm{d}A$ is the mean radius and the integral covers the protrusion portion only. In an ideal case, when the protrusion forms a perfect tube with radius $1/\tilde{c}_0$, $\gamma = 0$. On the other hand, when it forms a string of perfect spheres with radius $2/\tilde{c}_0$, $\langle r \rangle = \pi/2\tilde{c}_0$, then $\gamma = 1$. Thus γ indicates the protrusion shape continuously ranging from a string of beads to a cylinder.

The coupling constant $\tilde{c}_0$ controls the protrusion radius and the entire vesicle is constrained by the reduced volume v; as such the vesicle conformation strongly depends on both $\tilde{c}_0$ and v. In Fig. 1, using γ we plot the shape diagram in the $(\tilde{c}_0, v)$ plane. Starting from the top-left corner of the figure, a one-bead (bud) conformation exists; moving through each band, we see distinct conformations where one additional bead is added to or taken from the vesicle protrusion. Examples of conformation can be seen from the shapes plotted in Fig. 1. In the region $v < 0.3$, the vesicle adopts the shape of a long narrow capped cylinder. Likewise, in the region $\tilde{c}_0 > 10$, the protrusion forms a tubular structure.

The total energy F in Fig. 4(a) together with γ in Fig. 4(b) shows that there is a discontinuous transition each time the protrusion grows one additional bead. A series of shape transitions take place stage by stage between conformations having different number of beads; a similar behavior was reported from studying curvature-driven component sorting in lipid membranes[42]. At every transition point, the two branches of F cross and γ drastically jumps from the value at one state to another. Figure 4(c) illustrates the shape changes before and after the transition.

An interesting feature that can be deduced from Fig. 4(c) is within the parameter region $v < 0.4$. Soon after the entire vesicle becomes a string of beads, the vesicle's surface is uniformly covered by adhering particles, where $\phi = 1$ throughout the vesicle. As v is further lowered, the vesicle undergoes a transition from a seven-bead conformation to an eight-bead conformation and finally becomes a long narrow capped cylinder. The free energy plot F shows a behavior similar to that discussed in Ref. 38, in which a vesicle with a uniform spontaneous curvature was discussed; there the system undergoes a transition from two beads to three beads and finally becomes a long prolate.

In the above we mainly focused on the discussion of a system where $\tilde{c}_0 = 5.0$ in Figs. 4(b) and (c). As can be viewed from Fig. 4(a), for other $\tilde{c}_0$ similar sequences of stage-by-stage transitions exist. At the transition points, the magnitudes of free energy cusps become smaller in a greater-$\tilde{c}_0$ system. Especially in the small v region, the energy difference between two neighboring multi-pearling states containing n and $n+1$ beads is no longer large, if $n \gg 1$. These pearling-to-pearling and the final pearling-to-tube shape transitions appear much weaker within the same energy scale plotted in Fig. 4(a). This can be viewed from the color variations in Fig. 1 as well. The contrast of color between neighboring bands demonstrates the magnitude of the structural difference. For a $\tilde{c}_0$ as large as 14 (to the right potion of Fig. 1), as v varies, a few first steps of pearling-to-pearling transitions can be clearly identified but soon, the structural difference becomes very weak.

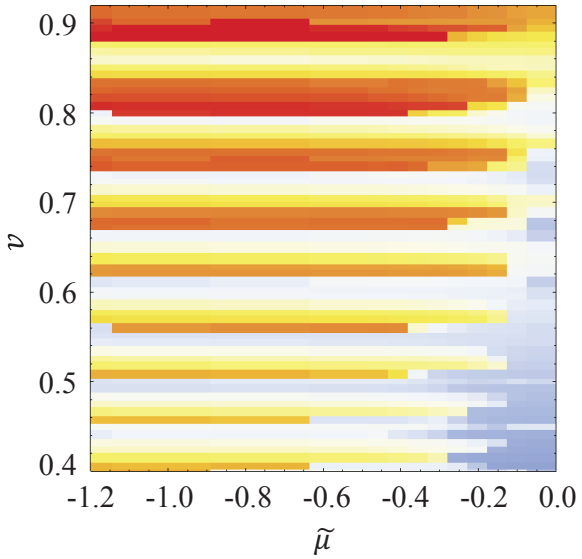

Fig. 5 Structure diagram in terms of the reduced volume v versus the reduced chemical potential $\tilde{\mu}$ for the reduced spontaneous curvature $\tilde{c}_0 = 7.6$. The color scheme is the same as the one in Fig. 1. The shapes of protrusion are affected by both v and $\tilde{\mu}$. Increasing $\tilde{\mu}$ transforms the membrane into a string of beads while the number of beads solely depends on v and $\tilde{c}_0$.

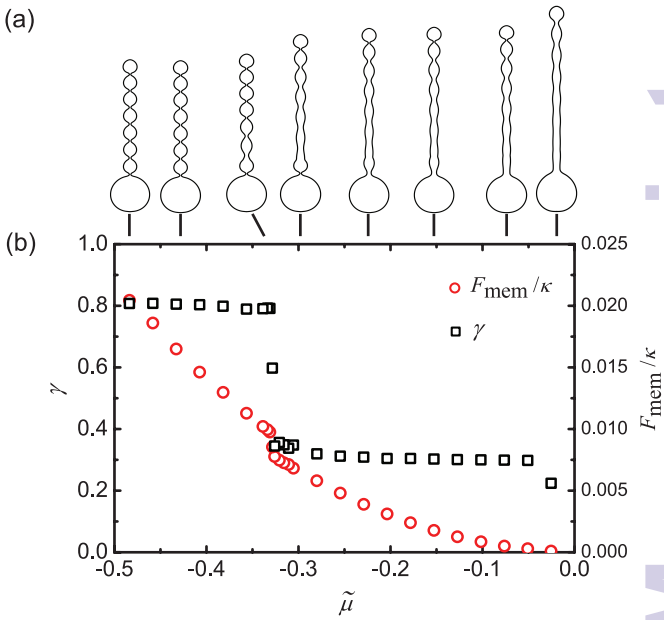

Fig. 6 (a) Membrane shape as well as (b) membrane energy $F_{\rm mem}$ and γ as functions of $\tilde{\mu}$ for $\tilde{c}_0 = 7.6$ and $v = 0.51$. At the reduced chemical potential $\tilde{\mu} = -0.34$, $F_{\rm mem}$ and γ exhibit a jump.

5 Tubulation-pearling transition

An example of the structure diagram in the $(\tilde{\mu}, v)$ plane with a fixed $\tilde{c}_0$ is displayed in Fig. 5. The stripe pattern again represents the value of γ and implies that the pearling structures of the vesicle is mainly determined by $\tilde{c}_0$ and v as long as $|\tilde{\mu}|$ is large enough. In the weak-$|\tilde{\mu}|$ region, there is a significant area on the diagram colored by light blue, where the protrusion part forms a tubular shape. Increasing $|\tilde{\mu}|$ generally drives the membrane into a pearling shape. This is because a larger $|\tilde{\mu}|$ prompts the system to take more membrane area from the mother vesicle, which stays in a spherical shape itself, to form the shape according to $\tilde{c}_0$ in protrusion. Forming spherical beads can accommodate the largest volume in the protrusion and enables more membrane area from the mother vesicle to adopt the shape according to $\tilde{c}_0$. Hence for a fixed v, a high $|\tilde{\mu}|$ area corresponds to the pearling regime.

To further demonstrate the effects of $\tilde{\mu}$ on a system with fixed v and $\tilde{c}_0$ in more details, we display an example of shape transformation from a tube-like structure to a pearl necklace in Fig. 6(a). The tube-like structure at a low $|\tilde{\mu}|$ gradually evolves into a shape with a hint of pearling when it reaches $|\tilde{\mu}| \simeq 0.34$ where a discontinuous transition takes place. Beyond $|\tilde{\mu}| \simeq 0.34$, a clearly-defined pearling structure is stabilized. Both the membrane energy in Eq. (2) and γ, to the left and right scales of Fig. 6(b) respectively, undergo an abrupt transition at the transition point. The value of γ is significantly larger in the pearling state than in the pre-pearling, tube-like state.

From the discussion in this and last sections, we can summarize the basic physical picture here. The adsorption energy is the drive force that enables the tubulation-pearling transition and stabilizes a structure. This changes the effective spontaneous curvature ϕc_0 as well as lowers the total adsorption energy. The parameters v and $\tilde{c}_0$ determines the structure of th stable states, such as the number of beads in a pearling state. By varying these two parameters, as demonstrated in the last section, various states are available.

6 Comparison with experiments

A dynamic tubulation/pearling process was presented in a series of fluorescence images by Yu and Granick [15]. The initial state was a GUV formed and stablized in a nanoparticle solution, displaying a spherical shape. At time $t = 0$, the nanoparticle solution outside GUV was diluted, and the initially adsorbed nanoparticles on the exterior surface started a desorbing process; structural transformation then took place. The adsorption area-fraction difference between interior and exterior surfaces can serve as the net ϕ in our model.

The process accompanies solvent filtration through the membrane surface, as such the enclosed volume is *not* constrained. The equilibrium state of a volume-constraint-free system can be deduced from the minimum in the F-v curve presented in, for example, Fig. 4. Before dilution, both membrane sides contain an almost equal amount of nanoparticles, i.e. $\phi = 0$; hence the spontaneous curvature term vanishes[15,22]. GUV takes an optimal shape corresponding to the bending-energy minimum, i.e, a sphere where $v = 1$[38] [see Fig. 7(a)].

Strictly speaking, our study here only concerns about the equilibrium states. The initial spherical GUV has an equilibrium radius $\sim 10\,\mu$m and the final equilibrium state containing pearls that have a radius $\sim 2.5\,\mu$m. Thus $\tilde{c}_0$ can be estimated from $10 \times 2/2.5 \sim 8.0$. In order to qualitatively explain the evolution of pearling kinetics observed in the above experiment, we assume that the nanoparticle desorption dynamics on the surface and solvent filtration across the membrane is slower than the membrane deformation response. In other words, during the pearling evolution, the vesicle is in a quasi-equilibrium state controlled by the time-dependent μ and v. If this assumption is false, the final pearling structure would quickly form without going through the intermediate states.

In the following, we examine a series of simulation results with $\tilde{c}_0 = 7.6$. After $t = 0$, once nanoparticles start to desorb from GUV's exterior surface, the system can be *effectively* described by a weak $|\tilde{\mu}|$ and prefers a smaller v. The solvent permeability across the membrane surface, on the other hand, prevents an immediate reduction of v. The GUV conformation now corresponds to Fig. 7(b). As the exterior nanoparticles further leave the surface (i.e., the effective $|\tilde{\mu}|$ increases) and solvent filtrates through the membrane (i.e., v is reduced), a tube starts to emerge and is elongated [Fig. 7(c)]. Progressively, more nanoparticles leave the exterior surface and the system is effectively in a $|\tilde{\mu}|$ region where a long tube forms, which contains some structures resembling the initial formation of beads [Fig. 7(d)]. At a certain stage the vesicle undergoes a tubulation-pearling transition. Finally, the equilibrated system reaches an energy minimum and becomes a necklace connecting a string of fifteen pearls, which is comparable to the number of final pearls formed in the experiment. The above qualitative description, of course, does not take the initial multiple protrusions seen in a real experiment into account.

Tsafrir *et al.* observed the pearling instability of a membrane tube by introducing hydrophilic polymers with hydrophobic side groups in the outside solvent[4]. They showed that the radius of pearls strongly depend on the adsorbing polymer concentration, justifying the idea of a concentration-coupled spontaneous radius, used in our model and in their work. Most equilibrium states of the current model contain a large-radius mother cell connected to a string of pearls with

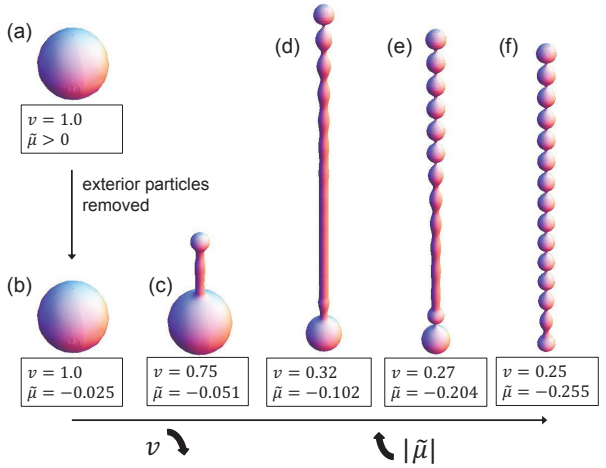

Fig. 7 Illustration of a transition path similar to the observation in a recent experiment[15]. All the shapes were obtained from free energy minimization for $\tilde{c}_0 = 7.6$.

almost *identical* small radius (Fig. 4). This is consistent with the final equilibrium state of the nanoparticle-induced pearling experiment[15]. In contrast, the final snapshot of Tsafrir *et al.*'s experiment (Fig. 1d of Ref. 4) displays a gradient of radius of the pearls from the large-radius mother cell to the smallest, un-explained by the current model.

Summary

A free-energy model is used to study the tubulation and pearling transition for a vesicle interacting with a particle solution. The mechanism responsible for generating the spontaneous curvature was described by a chemical potential, which controls the surface fraction affected by adsorbing particles. Two key physical effects were taken into account within the coarse-grained Helfrich model: change in the spontaneous curvature and the adsorption energy. Through minimization of the free energy, we show that two main types of structures are possible: a vesicle connected to a tubular or pearling protrusions. The morphology of protrusion depends on a subtle balance between the spontaneous curvature, the chemical potential, and the reduced volume.

Examining the structure of the free energy in Eq. 2, one could interpret it as a model for a two-component vesicle; the last term is just an energy penalty with a Lagrange multiplier $\tilde{\mu}$ to maintain the overall composition constant on the vesicle. Mixing entropy needs be considered in this case, and $\tilde{\mu}$ must be re-expressed as a function of the total composition ratio as the control parameter. We are, however, facing a dif-

ferent problem here where $\tilde{\mu}$, the adsorption energy between particles in the solution and the membrane surface, is the control parameter and dominates over the entropic effects. By solving this model, not only we demonstrate that tubulation and pearling are possible in such a simple model, but we also show that "phase" separation between the ϕ-rich and ϕ-poor regions can be completely driven by segregation of the coupled spontaneous curvatures in different domains.

Acknowledgement

Financial support from the Natural Sciences and Engineering Council of Canada is gratefully acknowledged. This work was made possible by the facilities of the Shared Hierarchical Academic Research Computing Network and Compute Canada.

References

1 I. Koltover, J. O. Rädler and C. R. Safinya, *Phys. Rev. Lett.*, 1999, **82**, 1991.
2 R. Bar-Ziv, T. Tlusty, E. Moses, S. A. Safran and A. Bershadsky, *Proc. Natl. Acad. Sci. USA*, 1999, **96**, 10140.
3 K. Farsad, N. Ringstad, K. Takei, S. R. Floyd, K. Rose and P. D. Camilli, *J. Cell Biol.*, 2001, **155**, 193.
4 I. Tsafrir, D. Sagi, T. Arzi, M.-A. Guedeau-Boudeville, V. Frette, D. Kandel and J. Stavans, *Phys. Rev. Lett.*, 2001, **86**, 1138.
5 I. Tsafrir, Y. Caspi, M. A. Guedeau-Boudeville, T. Arzi and J. Stavans, *Phys. Rev. Lett.*, 2003, **91**, 138102.
6 H. T. McMahon and J. L. Gallop, *Nature*, 2005, **438**, 590.
7 T. Itoh, K. S. Erdmann, A. Roux, B. Habermann, H. Werner and P. D. Camilli, *Dev. Cell*, 2005, **9**, 791.
8 M. Tokarz, B. Akerman, J. Olofsson, J.-F. Joanny, P. Dommersnes and O. Orwar, *Proc. Natl. Acad. Sci. USA*, 2005, **102**, 9127.
9 V. Vogel and M. Sheetz, *Nature Rev. Mol. Cell Biol.*, 2006, **7**, 265.
10 G. K. Voeltz, W. A. Prinz, Y. Shibata, J. M. Rist and T. A. Rapoport, *Cell*, 2006, **124**, 573.
11 J. Zimmerberg and M. M. Kozlov, *Nature Rev. Mol. Cell Biol.*, 2006, **7**, 9.
12 R. Dimova, S. Aranda, N. Bezlyepkina, V. Nikolov, K. A. Riske and R. Lipowsky, *J. Phys.: Cond. Matt.*, 2006, **18**, S1151.
13 Y. Roiter, M. Ornatska, A. R. Rammohan, J. Balakrishnan, D. R. Heine and S. Minko, *Nano Lett.*, 2008, **8**, 941.
14 W. Jiang, B. Y. Kim and J. T. Rutka, *Nat. Nanotecnol.*, 2008, **3**, 145.
15 Y. Yu and S. Granick, *J. Am. Chem. Soc.*, 2009, **131**, 14158–14159.
16 H. Ewers, W. Romer, A. E. Smith, K. Bacia, S. Dmitrieff, W. Chai, R. Mancini, J. Kartenbeck, V. Chambon, L. Berland, A. Oppenheim, G. Schwarzmann, T. Feizi, P. Schwille, P. Sens, A. Helenius and L. Johannes, *Nat. Cell Biol.*, 2010, **12**, 11.
17 J. C. Stachowiak, C. C. Hayden and D. Y. Sasaki, *Proc. Natl. Acad. Sci. USA*, 2010, **107**, 7781.
18 F. Thalman, V. Billot and C. M. Marques, *Phys. Rev. E*, 2011, **83**, 061922.
19 S. Zhang, A. Nelson and P. A. Beales, *Langmuir*, 2012, **28**, 12831.
20 R. Bar-Ziv and E. Moses, *Phys. Rev. Lett.*, 1994, **73**, 1392.
21 P. A. Pullarkat, P. Dommersnes, P. Fernandez, J.-F. Joanny and A. Ott, *Phys. Rev. Lett.*, 2006, **96**, 048104.
22 I. Gözen, C. Billerit, P. Dommersnes, A. Jesorka and O. Orwar, *Soft Matter*, 2011, **7**, 9706.
23 V. Frette, I. Tsafrir, M.-A. Guedeau-Boudeville, L. Jullien, D. Kandel and J. Stavans1, *Phys. Rev. Lett.*, 1999, **83**, 2465.
24 M. Müller, K. Katsov and M. Schick, *Phys. Rep.*, 2006, **434**, 113.
25 U. Seifert, *Advances in Physics*, 1997, **46**, 13.
26 U. Seifert, K. Berndl and R. Lipowsky, *Phys. Rev. A*, 1991, **44**, 1182.
27 L. Miao, F. B., R. M., M. Wortis and R. K. P. Zia, *Phys. Rev. A*, 1991, **43**, 5843.
28 W. Wiese, W. Harbich and W. Helfrich, *J. Phys.: Condens. Matter.*, 1992, **4**, 1647.
29 B. Bozic, S. Svetina, B. Žekš and R. Waugh, *Biophys. J.*, 1992, **61**, 963
30 U. Seifert, *Phys. Rev. Lett.*, 1993, **70**, 1335.
31 P. Nelson, T. Powers and U. Seifert, *Phys. Rev. Lett.*, 1995, **74**, 3384.
32 F. Campelo, J.-M. Allain and M. B. Amar, *Europhys. Lett.*, 2007, **77**, 38006.
33 F. Campelo and A. Hernández-Machado, *Phys. Rev. Lett.*, 2007, **99**, 088101.
34 F. Campelo and A. Hernández-Machado, *Phys. Rev. Lett.*, 2008, **100**, 158103.
35 R. Lipowsky and H. G. Döbereiner, *Europhys. Lett.*, 1998, **43**, 219.
36 P. Canham, *J. Theor. Biol.*, 1970, **26**, 61.
37 W. Helfrich, *Z. Natureforsch. C*, 1973, **28**, 693–703.
38 U. Seifert, K. Berndl and R. Lipowsky, *Phys. Rev. A*, 1991, **44**, 1182–1202.
39 W. T. Góźdź, *Langmuir*, 2004, **20**, 7385–7391.
40 W. T. Góźdź, *J. Phys. Chem. B*, 2005, **109**, 21145.
41 W. T. Góźdź, *J. Chem. Phys.*, 2011, **134**, 024110.
42 W. T. Góźdź, *J. Chem. Phys.*, 2012, **137**, 015101.
43 H. Jiang and T. R. Powers, *Phys. Rev. Lett.*, 2008, **101**, 018103.
44 J. Z. Y. Chen, *Phys. Rev. E*, 2012, **85**, 061910.
45 J. Z. Y. Chen, *Phys. Rev. E*, 2012, **86**, 041904.
46 O.-Y. Zhong-can and W. Helfrich, *Phys. Rev. A*, 1989, **39**, 5280–5288.
47 L. Miao, U. Seifert, M. Wortis and H.-G. Döbereiner, *Phys. Rev. E*, 1994, **49**, 5389.
48 S. Q. Cao, G. H. Wei and J. Z. Y. Chen, *Phys. Rev. E*, 2011, **84**, 050901(R).
49 R. H. Byrd, P. Lu and J. Nocedal, *SIAM J. Sci. Comput.*, 1995, **16**, 1190.

TOC FIGURE: Model of vesicle tubulation and pearling induced by adsorbing particles

Yucheng Su and Jeff Z. Y. Chen

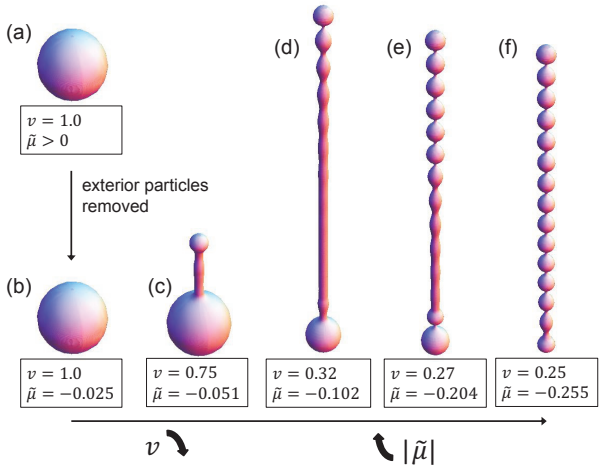

A transition path sequence is found, similar to the observation in a recent experiment, for the tubulation and pearling transition of a vesicle immersed in a nanoparticle solution.